

AnthroTAP: Learning Point Tracking with Real-World Motion

Inès Hyeonsu Kim^{1,3*} Seokju Cho^{1*} Jahyeok Koo¹ Junghyun Park¹
 Jiahui Huang² Honglak Lee^{3,4} Joon-Young Lee² Seungryong Kim¹

¹KAIST AI ²Adobe Research ³University of Michigan ⁴LG AI Research

<https://cvlab-kaist.github.io/AnthroTAP/>

Abstract

Point tracking models often struggle to generalize to real-world videos because large-scale training data is predominantly synthetic—the only source currently feasible to produce at scale. Collecting real-world annotations, however, is prohibitively expensive, as it requires tracking hundreds of points across frames. We introduce **AnthroTAP**, an automated pipeline that generates large-scale pseudo-labeled point tracking data from real human motion videos. Leveraging the structured complexity of human movement—non-rigid deformations, articulated motion, and frequent occlusions—AnthroTAP fits Skinned Multi-Person Linear (SMPL) models to detected humans, projects mesh vertices onto image planes, resolves occlusions via ray-casting, and filters unreliable tracks using optical flow consistency. A model trained on the AnthroTAP dataset achieves state-of-the-art performance on TAP-Vid, a challenging general-domain benchmark for tracking any point on diverse rigid and non-rigid objects (e.g., humans, animals, robots, and vehicles). Our approach outperforms recent self-supervised teacher-student models trained on vastly larger real datasets, while requiring only one day of training on 4 GPUs. AnthroTAP shows that structured human motion offers a scalable and effective source of real-world supervision for point tracking. Code and datasets will be made publicly available.

1. Introduction

Accurately tracking points on an object’s surface within a video, a task known as point tracking [12, 14–16, 22, 27, 28, 54], has become important for various applications, including robotics [4, 61, 67, 70], visual odometry [9, 51], 3D [62, 63] or 4D reconstruction [2, 18, 30, 53, 65], video editing [19, 25], and motion segmentation [23, 29].

Despite its growing significance, acquiring the extensive and diverse real-world data remains a significant challenge. Specifically, manually annotating point trajectories

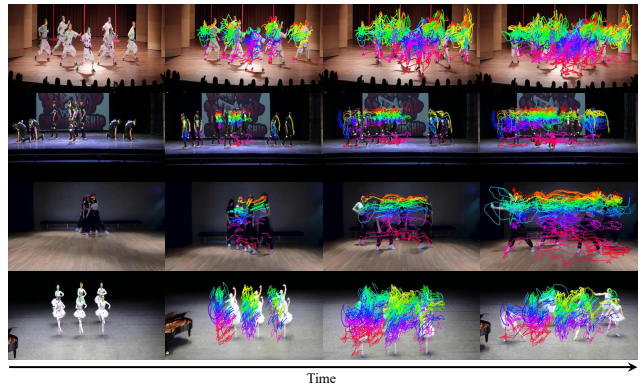


Figure 1: Visualization of videos annotated with our pipeline. In this example, we visualize trajectories extracted using our pipeline using videos from [58]. These examples highlight the complexity of human crowd movement, including both intra-person and inter-person interactions. We leverage this complexity as a source of supervision for training point tracking models.

in video sequences is extremely labor-intensive and time-consuming [14, 71], making it a major bottleneck for acquiring real training data. Consequently, the limited availability of real-world training data often restrict the ability of current tracking models to generalize effectively across the diverse real-world scenarios [16, 27]. Although synthetic datasets [21, 42, 71] can be generated at scale, they often fail to capture the complex visual characteristics inherent to real-world scenarios.

Several recent works attempt to address this issue by utilizing self-distillation on real videos [16, 27]; however, these methods often demand extensive computational resources and vast datasets (e.g., 15M videos with 256 GPUs in Doersch et al. [16]) and often show limited improvement, possibly due to the weak supervision signal derived from the model itself. In addition, self-distillation frameworks may suffer from confirmation bias [56]. As a result, efficiently training point tracking models with realistic video data remains an open challenge.

Our key insight is that human motion offers a unique

combination of properties: by distilling knowledge from human mesh fitting models, we can automatically establish reliable point correspondences, leveraging real-world data characteristics and inherent complexities such as non-rigid deformations, articulated movements, and frequent occlusions to generate complex and effective pseudo-labeled training data for point tracking without manual annotation. For instance, as an individual walks, dances, or turns, this point can be obscured by limbs, or hidden by other articulated bodies in a crowded scene. When multiple people are present, the complexity increases further, as exemplified in Figure 1. In addition, videos capturing human activity reflect this real-world richness, featuring motion blur, varying lighting conditions, and reflective surfaces, all of which are highly difficult to replicate authentically in simulated environments. We believe that these challenges from human motion with real-world visual characteristics provides essential training signals for robust trackers. Furthermore, as shown in [13, 68], point motion carries an inherent 3D structure. Given that 2D trajectories are projections of such 3D motion, leveraging the underlying human 3D geometry provides a natural and effective way to improve 2D tracking accuracy.

To this end, we introduce **AnthroTAP**, a pseudo-labeling pipeline that distills knowledge from human motion to automatically generate real-world point tracking training data. AnthroTAP initially fits the SMPL model to humans detected in each video frame using a pre-trained Human Mesh Recovery (HMR) method [17], producing a 3D mesh for each person. The trajectories of these 3D mesh vertices are projected onto the 2D image plane, forming initial pseudo-trajectories. To manage occlusions, we apply a ray-casting leveraging the 3D mesh structure to estimate point visibility, considering both self-occlusion and inter-person occlusion. Finally, to enhance pseudo-label reliability, we introduce a filtering stage based on optical flow consistency [43] between adjacent frames.

We validate our approach by training a point tracking model [12] using the generated pseudo-labels. The effectiveness of our data generation pipeline is demonstrated by the model’s performance in complex real-world scenarios, achieving state-of-the-art results on the TAP-Vid benchmark [14], which is a standard evaluation for tracking any point on diverse, real-world videos of general objects. Our method outperforms CoTracker3 [27], which utilizes $11\times$ more training data, and BootsTAPIR [16], which uses approximately $10,000\times$ more videos. This underscores the advantage of leveraging complex human motion for efficient and effective point tracking. Moreover, unlike previous works such as BootsTAPIR [16] and CoTracker3 [28] that uses proprietary videos, our dataset is non-proprietary and can be fully open-sourced, contributing valuable resources to the research community.

Our contributions are summarized as follows:

- Introduces a simple yet effective approach to leverage real-world training data for point tracking by distilling knowledge from human motion, enabling automatic generation of pseudo-labeled datasets with strong supervision signals that capture complex motion patterns and real-world visual characteristics.
- Leverages the inherent complexities of human motion from videos, using human model fitting and 3D geometry, to automatically generate complex and diverse pseudo-labeled datasets for training robust point trackers.
- Achieves state-of-the-art point tracking performance with significantly less training data, utilizes a non-proprietary dataset that can be open-sourced, offering a valuable contribution to the point tracking community.

2. Related work

Point tracking. PIPs [22] iteratively refines point estimations by constructing local correlation maps, inspired by optical flow methods such as RAFT [59]. TAPIR [15] extends this idea by combining per-frame initialization from TAP-Net [14] with iterative refinement inspired by PIPs. CoTracker [28] learns to track multiple points jointly to enhance reliability. LocoTrack [12] introduces a local 4D correlation to establish better correspondence within videos.

Despite recent advances in model architectures for track refinement, existing methods [1, 11, 12, 14, 15, 22, 34, 36, 37, 49] predominantly rely on synthetic data [21, 42, 71] during training, which can limit the robustness of point tracking in complex real-world scenarios. To alleviate this issue, Chrono [32] leverages representations learned by DI-NOv2 [46], a model pre-trained on large-scale real-world datasets. Similarly, BootsTAP [16] and CoTracker3 [27] incorporate unlabeled real-world data via self-training to further reduce dependency on synthetic data. However, these methods do not explicitly model the distinctive complexities found in human motion, such as significant non-rigid deformations, diverse textures from clothes, and frequent occlusions arising from interactions within and between individuals. In contrast, our approach specifically targets learning from human motion, which includes these challenging yet commonly occurring real-world phenomena.

Point tracking datasets and benchmarks. Kubric [21] is a data generator that creates synthetic scenes for various tasks [50, 52, 55], including point tracking. While most point tracking methods [12, 15, 28, 34, 37] are trained solely on the Kubric dataset, it features limited motion, primarily consisting of objects falling onto the floor. TAP-Vid [14] provides manual annotations on unlabeled real-world datasets [31, 35, 48]. However, manually annotating point tracks in real videos is extremely time-consuming, making it impractical to scale such efforts for generating training data. DriveTrack [3] explores automated dataset

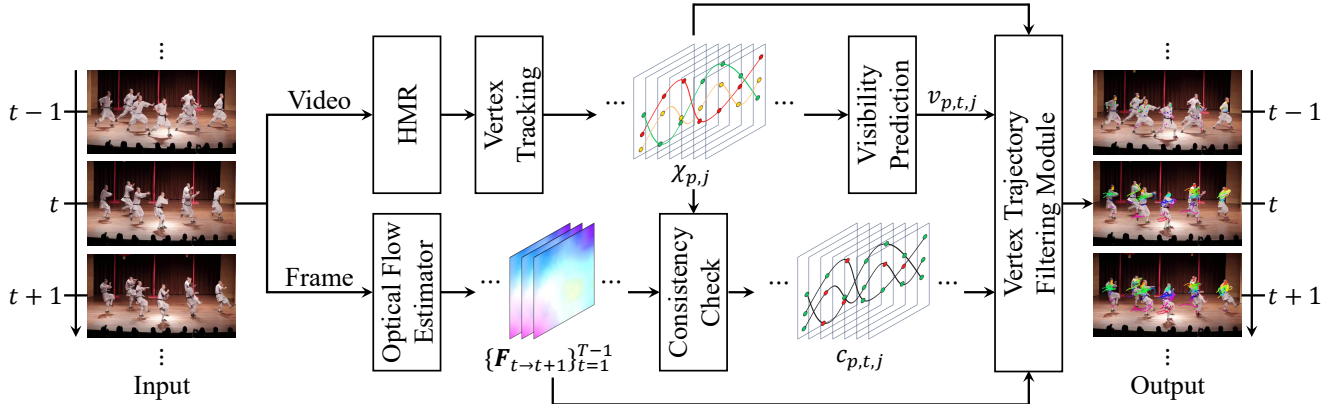


Figure 2: Overall pipeline. We extract human meshes using an off-the-shelf human mesh recovery model [17], and track points by projecting the mesh vertices. We also determine point visibility using ray-casting. In parallel, we extract optical flow [66] and retain only reliable flow using forward-backward consistency [43]. Finally, we filter the trajectories by checking the consistency between the optical flow and the trajectories generated from the human mesh.

generation in driving scenes [57]; however, the resulting trajectories lack complexity due to relatively simple vehicle motions, no deformation or articulated motion.

Human Mesh Recovery. Goal of Human Mesh Recovery (HMR) is to estimate a full 3D human mesh from a monocular 2D image or video. SMPL [40] proposes an optimization method for parameterized human pose and shape. Early works [6, 33] leverage 2D joint prediction obtained from off-the-shelf 2D pose estimation models [7, 69] and predict 3D body model defined by SMPL. With the advancement of 3D body model prediction from single images, several video-based approaches [17, 20] have been developed. TokenHMR [17] introduces tokenized representation for human pose and achieves state-of-the-art accuracy on multiple in-the-wild 3D benchmarks. We aim to utilize the 3D prior from the Human Mesh Recovery model, to automatically generate complex pseudo-labeled datasets and improve point trackers with the annotated datasets.

3. Method

The development of robust point tracking models often limited by the scarcity of large-scale, diverse real-world training data. This scarcity stems from the prohibitively time-consuming and labor-intensive nature of manually annotating point trajectories in real-world videos [14], making large-scale annotation infeasible. Although synthetic datasets [21, 26, 42, 71] can be generated at scale, they often fail to capture key characteristics of real-world scenes, such as complex motions and lighting, realistic appearance variations, and dynamic occlusions. Recent efforts have attempted to overcome this limitation using self-training approaches on unlabeled real videos [16, 27]. While promising, these methods suffer from weak supervision signals and often rely on random or heuristic trajectory sampling, limiting their training efficiency.

To address this challenge, we propose **AnthroTAP**, a pseudo-labeling pipeline that enables leveraging human motion as a natural source of rich supervision for point tracking. Human activities inherently involve complex visual and geometric phenomena, such as non-rigid deformations, articulated motion, occlusions, and diverse clothing appearances, as shown in Figure 1. To benefit from these, we leverage point trajectory across time, using the Skinned Multi-Person Linear (SMPL) model [39], a parametric 3D representation of the human body to generate complex pseudo-labels. Since each vertex on the SMPL mesh corresponds to a fixed anatomical location, it enables consistent and temporally stable point trajectories to be generated from human-centric videos.

To further improve the reliability of the resulting pseudo-labels, we introduce a refinement step based on short-range optical flow consistency, a method proven effective over short temporal windows [11]. This process filters out erroneous trajectory segments caused by mesh fitting errors or occlusions from objects not modeled by SMPL, such as furniture or scene clutter.

An overview of our full pipeline is shown in Figure 2, and the following sections describe each stage in detail, from initial pseudo-label generation to final trajectory refinement.

3.1. Point tracking with human mesh models

Our pseudo-label generation process is founded upon utilizing the SMPL model [39] as a representation for human bodies. For each detected person, indexed by p , in a video frame t , the SMPL model defines a 3D body mesh $\mathcal{M}_{p,t}$ composed of N_v vertices. This mesh is parameterized by low-dimensional 3D human shape parameters $\beta_p \in \mathbb{R}^{D_\beta}$ (typically assumed constant for a person across a sequence) and 3D human pose parameters $\theta_{p,t} \in \mathbb{R}^{D_\theta}$. D_β represents the dimensionality of the identity-specific shape space, while

D_θ corresponds to the dimensionality of the pose space, capturing body articulation and global orientation. The function $M(\beta_p, \theta_{p,t})$ maps these parameters to a set of 3D vertex locations $\{\mathbf{v}_{p,t,j} \in \mathbb{R}^3\}_{j=1}^{N_v}$.

To obtain these SMPL parameters from video frames, we employ a pre-trained video Human Mesh Recovery (HMR) method [17]. Leveraging a strong human prior, the model can reliably track and reconstruct human bodies even under motion blur, extreme motion, or occlusions, which are scenarios where conventional point tracking methods often fail. Given an input video $\{I_t\}_{t=1}^T$, where T is the number of frames, the HMR model processes the video and outputs the estimated shape parameters β_p and pose parameters $\theta_{p,t}$ for each detected person p . When the HMR process yields reliable estimations across a sequence of frames, the temporal sequence of corresponding 3D vertex locations $\{\mathbf{v}_{p,t,j}\}_{t \in \mathcal{T}_{p,j}}$ for a specific vertex index j on person p provides an initial 3D trajectory estimation for a point on the human body surface. Here, $\mathcal{T}_{p,j}$ represents the set of frame indices for which vertex j of person p is successfully tracked.

These estimated 3D vertex locations are subsequently projected onto the 2D image plane to generate corresponding 2D pseudo-trajectories. Let $\Pi : \mathbb{R}^3 \rightarrow \mathbb{R}^2$ denote the camera projection function, which maps a 3D point in camera coordinates to its 2D pixel coordinates using known camera intrinsic and extrinsic parameters. The 2D pseudo-trajectory for vertex j of person p is thus given by $\mathcal{X}_{p,j} = \{\mathbf{x}_{p,t,j} = \Pi(\mathbf{v}_{p,t,j}) \mid t \in \mathcal{T}_{p,j}\}$.

Visibility prediction with ray casting. Accurate prediction of point visibility is crucial for generating reliable pseudo-labels, as points that become occluded, either by parts of the same body (self-occlusion) or by other humans or scene elements (inter-object occlusion), cannot provide dependable supervision signals. Given that we have explicit 3D mesh representations for all detected humans, we can geometrically reason about occlusions among them. We determine the estimated visibility $v_{p,t,j}$ for each 2D pseudo-labeled point $\mathbf{x}_{p,t,j}$ based on the visibility status of its corresponding 3D vertex $\mathbf{v}_{p,t,j}$. The visibility $v_{p,t,j}$ is a binary indicator, where $v_{p,t,j} = 1$ signifies that the point is estimated to be visible with respect to all modeled human meshes, and $v_{p,t,j} = 0$ signifies that it is estimated to be occluded by any part of any modeled human mesh.

We determine visibility using a ray casting approach within the estimated 3D scene. For each vertex $\mathbf{v}_{p,t,j}$ of person p at frame t , we cast a ray from the camera’s optical center \mathbf{c} towards $\mathbf{v}_{p,t,j}$. This ray can be parameterized as $\mathbf{r}(s) = \mathbf{c} + s(\mathbf{v}_{p,t,j} - \mathbf{c})$ for $s \geq 0$. We then identify all intersection points between this ray and the triangular faces of all human meshes $\mathcal{M}_{p',t}$ present in frame t , considering all persons p' from 1 to $N_{P,t}$. Let $s_{\text{int},k}$ be the parameter s for the k -th intersection point. The vertex $\mathbf{v}_{p,t,j}$ is considered visible ($v_{p,t,j} = 1$) if and only if the minimum s value

among all such intersection points is greater than or equal to 1. This implies that no part of any modeled human mesh intersects the ray segment $(\mathbf{c}, \mathbf{v}_{p,t,j})$ strictly before $\mathbf{v}_{p,t,j}$ itself.

Conversely, the vertex $\mathbf{v}_{p,t,j}$ is considered occluded ($v_{p,t,j} = 0$) if the closest intersection point along the ray (the one with the minimum $s_{\text{int},k}$) is with a triangle belonging to any human mesh surface, and that intersection is strictly closer to the camera than $\mathbf{v}_{p,t,j}$ itself, i.e., $\min_{k, \forall p'}(s_{\text{int},k}) < 1$. This ray-triangle intersection testing is efficiently implemented using the Möller-Trumbore algorithm [44], which can be significantly accelerated on modern GPUs. Note that this ray casting method accounts for occlusions by the modeled human bodies (both self and inter-person) and does not detect occlusions by other arbitrary scene objects. Limitations regarding occlusions by non-modeled scene elements are addressed in the subsequent filtering stage.

3.2. Supervised training with pseudo-labels

Vertex projection and ray casting for visibility prediction yield a collection of refined 2D point trajectories $\mathcal{X}_{p,j}$ with associated with visibility labels $v_{p,j}$. These trajectories serve as additional supervision for existing point tracking models [12, 27], and we simply apply each model’s original training loss. To further improve the quality of our pseudo-labeled human tracks, we introduce an additional optical flow-based filtering during the training that identifies and removes unreliable trajectory segments.

Optical-flow based trajectory filtering. Although modern HMR methods are generally robust, they still fail under extreme poses or occlusions. Since optical flow [59] provides accurate short-term motion cues, we compare the HMR-predicted motion of each tracked point with the corresponding flow-derived displacement.

For each trajectory, we identify transitions whose motion disagrees with the optical flow beyond a normalized threshold, where a forward-backward consistency check is used to ensure that the sampled flow is locally reliable. We then compute the fraction of erroneous transitions, considering only frames where both the HMR visibility and optical-flow reliability conditions are met. If this ratio exceeds a preset limit, the entire trajectory is discarded; otherwise, only the inconsistent transitions are removed. This process ensures that the final training set contains fewer but much more accurate pseudo-labels, which is preferable for learning a robust point tracker. The full details can be found in Sec. C of the supplementary material.

Table 1: Quantitative results on TAP-Vid benchmark [14] and RoboTAP [61]. LocoTrack-B, trained with our approach, shows a significant performance improvement across all metrics and datasets. Furthermore, *in terms of position accuracy ($< \delta_{avg}^x$), our model achieves the best performance on every dataset.* We use a training dataset that is $11\times$ smaller than CoTracker3 [27] in terms of the number of videos, and $1,000\times$ smaller than the dataset used in BootsTAPIR [16] in terms of the number of training frames. Kub refers to the Kubric dataset [21], while Kub64 refers to the dataset rendered in Karaev et al. [27]. Both Kub and Kub64 are synthetic datasets.

Method	Training Dataset	DAVIS First			DAVIS Strided			Kinetics First			RoboTAP First [61]		
		AJ	$< \delta_{avg}^x$	OA	AJ	$< \delta_{avg}^x$	OA	AJ	$< \delta_{avg}^x$	OA	AJ	$< \delta_{avg}^x$	OA
Models evaluated at 256×256 resolution													
OmniMotion [64]	-	-	-	-	51.7	67.5	85.3	-	-	-	-	-	-
Dino-Tracker [60]	-	-	-	-	62.3	78.2	87.5	-	-	-	-	-	-
TAPNet [14]	Kub	33.0	48.6	78.8	38.4	53.1	82.3	38.5	54.4	80.6	-	-	-
TAPIR [15]	Kub	58.5	70.0	86.5	61.3	73.6	88.8	49.6	64.2	85.0	59.6	73.4	87.0
Online TAPIR [61]	Kub	56.2	70.0	86.5	-	-	-	51.5	-	-	-	-	-
TAPTR [37]	Kub	63.0	76.1	<u>91.1</u>	66.3	79.2	<u>91.0</u>	49.0	64.4	85.2	60.1	75.3	86.9
TAPTRv2 [36]	Kub	<u>63.5</u>	75.9	91.4	66.4	78.8	91.3	49.7	64.2	85.7	-	-	-
TAPTRv3 [49]	Kub	63.2	76.7	91.0	-	-	-	<u>54.5</u>	<u>67.5</u>	88.2	-	-	-
BootsTAPIR [16]	Kub+15M	61.4	74.0	88.4	66.2	78.5	90.7	54.6	68.4	<u>86.5</u>	64.9	80.1	86.3
LocoTrack [12]	Kub	63.0	75.3	87.2	<u>67.8</u>	<u>79.6</u>	89.9	52.9	66.8	85.3	62.3	76.2	<u>87.1</u>
Anthro-LoCoTrack (Ours)	Kub+1.4K	64.8	77.3	89.1	69.0	81.0	90.8	53.9	68.4	86.4	<u>64.7</u>	<u>79.2</u>	88.4
Improvement over baseline		+1.8	+2.0	+1.9	+1.2	+1.4	+0.9	+1.0	+1.6	+1.1	+2.4	+3.0	+1.3
Models evaluated at 384×512 resolution													
PIPs [22]	FT [42]	42.2	64.8	77.7	52.4	70.0	83.6	-	-	-	-	-	-
CoTracker2 [28]	Kub	62.2	75.7	89.3	65.9	79.4	<u>89.9</u>	48.8	64.5	85.8	-	-	-
Track-On [1]	Kub	<u>65.0</u>	<u>78.0</u>	<u>90.8</u>	-	-	-	53.9	67.3	<u>87.8</u>	-	-	-
CoTracker3 (online) [27]	Kub64+15K	64.4	76.9	91.2	-	-	-	54.7	67.8	87.4	-	-	-
CoTracker3 (offline) [27]	Kub64+15K	63.8	76.3	90.2	-	-	-	55.8	<u>68.5</u>	88.3	-	-	-
LocoTrack [12]	Kub	64.8	77.4	86.2	<u>69.4</u>	<u>81.3</u>	88.6	52.3	66.4	82.1	-	-	-
Anthro-LoCoTrack (Ours)	Kub+1.4K	65.9	78.9	87.3	71.1	82.9	90.3	<u>54.8</u>	68.6	85.3	-	-	-
Improvement over baseline		+1.1	+1.5	+1.1	+1.7	+1.6	+1.7	+2.5	+2.2	+3.2	-	-	-

4. Experiments

4.1. Experimental setup

Dataset construction. We use the pre-trained TokenHMR [17] model for human mesh recovery and SEA-RAFT [66] for obtaining optical flow. To construct our training dataset, we use 1.4K videos from the Let’s Dance dataset [8], which includes a diverse range of dance performances, from solo acts to multi-person scenes. *Unlike BootsTAP [16] or CoTracker3 [16], our training videos are entirely non-proprietary.* This makes the training and annotation process fully reproducible, which we believe will make a valuable contribution to the point tracking community.

Training details. We fine-tune the pre-trained LocoTrack [12] base model using AnthroTAP-annotated Let’s Dance dataset, which called Anthro-LD. During fine-tuning, we randomly sample data from our dataset and Kubric Panning MOVi-E [15] with equal probability. When training with our dataset, we do not supervise the occlusion prediction for points identified as occluded, as we intentionally filter the dataset for high precision. We augment the filtered dataset using affine transformations, following the approach used in BootsTAP [16].

Optimization is performed using AdamW [41], with the learning rate of 3×10^{-4} and weight decay set to 1×10^{-3} .

The model is trained for 50K steps. We employ a cosine learning rate schedule with a 1000-step warmup, and apply gradient clipping with a maximum norm of 1.0. Training is conducted with a batch size of 1 per GPU, using 4 NVIDIA A6000 GPUs, and converges within 1 day. This is significantly more efficient compared to CoTracker3, which uses 32 A100 80GB GPUs for training, and BootsTAPIR, which uses 256 A100 GPUs. For each batch, we randomly sample 256 tracks and use a resolution of 256×256 .

Evaluation protocol. We use the TAP-Vid [14] benchmark to evaluate our model trained on Anthro-LD. We also evaluate our model on the RoboTAP dataset [61], a real-world robot dataset featuring videos of robotic manipulation tasks. The benchmark uses two evaluation modes based on how query points are selected: the **First** setup samples the query point from the first visible frame of each trajectory, whereas the **Strided** setup samples the query point every five timesteps along the trajectory. For evaluation, we use the following metrics, proposed in Doersch et al. [14]: Average Jaccard (AJ), position accuracy ($< \delta_{avg}^x$), and Occlusion Accuracy (OA).

Trajectory metrics. To characterize the motion captured by our pseudo-labeled trajectories $\mathcal{X}_{p,j}$, we use simple metrics for measuring their complexity and diversity. Trajectory complexity is measured using the mean angular accelera-

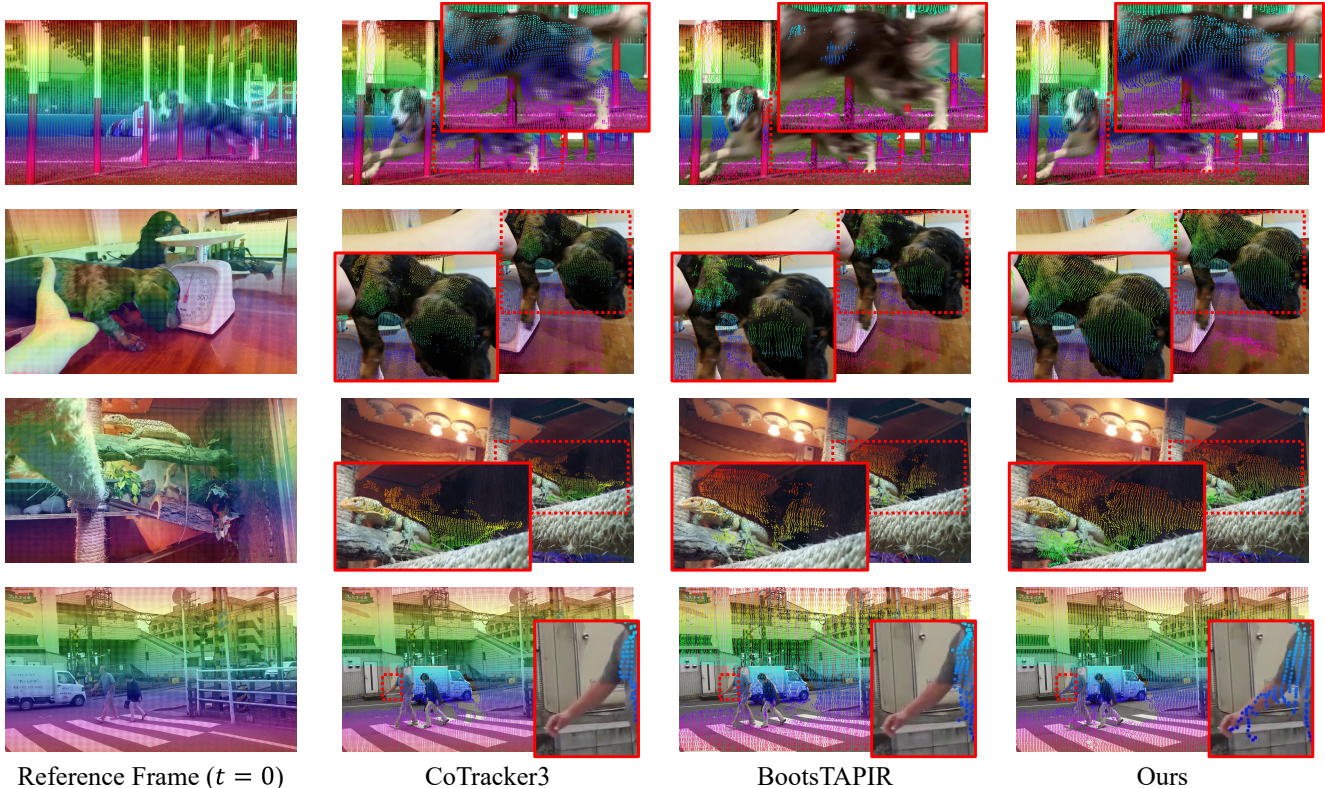


Figure 3: Qualitative results on the videos from DAVIS dataset [48]. We present comparisons with CoTracker3 [27] and BootsTAPIR [16]. Anthro-LoCoTrack (Ours) consistently demonstrates strong performance on highly deformable objects and severe occlusions.

tion, which reflects how sharply and frequently a trajectory changes direction, computed over all contiguous visible segments. Diversity is assessed by evaluating how much individual trajectories deviate from a mean centered trajectory within each video, providing a measure of shape variability independent of absolute positions. Together, these metrics summarize how dynamic and varied the trajectories are across the dataset. Refer to Sec. D of the supplementary material for details.

4.2. Main results

Quantitative comparisons. In Table 1, we present quantitative results on the TAP-Vid benchmark using the LocoTrack [12] base model trained with the dataset generated by our pipeline. Our primary comparisons are against BootsTAPIR [16] and CoTracker3 [27] on the DAVIS [47] and Kinetics [31], which consist of real-world videos. BootsTAPIR and CoTracker3 were trained on 15 million and 15,000 real videos respectively, whereas our model is trained on just 1,400 videos.

Despite this significant difference in training data scale, our method achieves notable performance gains. On the DAVIS First subset, our model surpasses BootsTAPIR by 3.3 percentage points on the $< \delta_{avg}^x$, demonstrating the data efficiency of our approach. Additionally, it outperforms

CoTracker3 by 2.0 percentage points on the same metric.

Qualitative comparisons. In Figure 3, we visually compare the results of CoTracker3 [27], BootsTAPIR [16], and LoCoTrack trained with our method. Our model demonstrates more robust tracking performance even in drastic deformation and severe occlusions. Refer to Sec. B of the supplementary material for additional visualization.

4.3. Ablation and analysis

Can training on human points generalize to non-human points? In Table 2, we investigate this question by splitting the query points in the TAP-Vid-DAVIS dataset into human and non-human categories, and comparing the performance gain in each group relative to the baseline. We use Mask2Former [10] to identify points on humans. The results show that the performance improvements are significant for both human and non-human points, with an even greater boost observed for non-human points.

Comparison with self-training strategy of CoTracker3 on identical data. Table 3 compares our approach with the self-training strategy of CoTracker3 [27] on identical data. We fine-tuned the Kubric-pretrained CoTracker3 baseline on the Let’s Dance dataset [8], the same data our pipeline employs, via two methods: the original self-training from CoTracker3, and fine-tuning with pseudo-labels from AnthroTAP. This

Table 2: Can training on human points generalize to non-human points? To answer this question, we compare the performance by grouping query points on humans and non-human regions separately in TAP-Vid-DAVIS dataset [14]. Our method shows greater improvement on non-human points.

Benchmark	Method	AJ	$< \delta_{avg}^x$	OA
DAVIS (Human Only)	LocoTrack	50.7	42.4	57.8
	Anthro-LoCoTrack (Ours)	51.2 (+0.5)	43.3 (+0.9)	58.6 (+0.8)
DAVIS (Non-Human)	LocoTrack	58.8	73.1	83.9
	Anthro-LoCoTrack (Ours)	60.8 (+2.0)	75.2 (+2.1)	85.3 (+1.4)

Table 3: Comparison to self-training method introduced in CoTracker3 using the same video. We compare our pipeline with self-training introduced in Karaev et al. [27]. **(I)** CoTracker3 model trained on Kubric [21]. **(II)** fine-tunes the model on the Let’s Dance (LD) dataset using the self-training introduced in the paper. **(III)** trains CoTracker3 model using our pipeline. Our method shows greater performance boost than self-training introduced in CoTracker3.

	Model	Train Strategy	Dataset	DAVIS		
				AJ	$< \delta_{avg}^x$	OA
(I)	CoTracker3	Supervised	Kubric	63.8	76.3	90.2
(II)	CoTracker3	Self-training	LD [8]	64.2 (+0.4)	76.5 (+0.2)	89.6 (-0.6)
(III)	CoTracker3	AnthroTAP (Ours)	Anthro-LD	65.0 (+1.2)	77.3 (+1.0)	90.7 (+0.5)

Table 4: Comparison of track complexity and diversity with existing datasets. Our dataset exhibits significantly higher complexity and substantially greater diversity compared to another real dataset, DriveTrack.

Training Dataset	Data Type	Traj Metrics	
		Complexity	Diversity
DriveTrack [3]	Real	0.4396	0.0073
PointOdyssey [71]	Synthetic	0.5222	0.1597
Kubric [21]	Synthetic	0.1772	0.1165
Anthro-LD (Ours)	Real	1.2492	0.1008

allowed a direct comparison of both data utilization strategies on the same baseline and data.

Results in Table 3 show self-training by CoTracker3 yielded marginal baseline improvement on Let’s Dance. In contrast, pseudo-labels from AnthroTAP achieved significantly better performance, demonstrating that the quality of training signals from real-world data is important, not merely the use of such data.

Comparative analysis on trajectory complexity and diversity. In Table 4, we provide a comparative analysis of prevalent point tracking training datasets, focusing on trajectory complexity and diversity. We quantify trajectory complexity using the mean angular acceleration for each trajectory, thereby accounting for variations in direction. Trajectory diversity is assessed on a per-video basis by computing the mean standard deviation within each video. Anthro-LD, the Let’s Dance dataset [8] annotated using the AnthroTAP pipeline, shows the highest values for complexity and demonstrates greater diversity compared to other real-world datasets, such as DriveTrack [3].

Comparing real-world pseudo-GT with synthetic perfect GT. In Table 5, we investigate the relative importance of GT

Table 5: Comparison of models trained using point tracks sampled from synthetic human videos. The human points sampled from synthetic human videos do not provide a significant improvement over the baseline.

Method	Datasets	DAVIS		
		AJ	$< \delta_{avg}^x$	OA
LocoTrack (256×256)	Kub64	63.0	75.3	87.2
LocoTrack + BlinkVision [38]	Kub64 + 1.4K	64.2	76.4	88.8
LocoTrack + Ours	Kub64 + 1.4K	64.8	77.3	89.1

accuracy versus real-world training signals using BlinkVision [38], a synthetic human mesh generator providing perfect GT with human motion. We train LocoTrack on three configurations: baseline, BlinkVision (perfect GT, synthetic), and AnthroTAP annotated dataset (pseudo-GT, real-world). Results show BlinkVision improves over baseline, but AnthroTAP annotated dataset achieves substantially larger gains despite pseudo-GT labels. Results show BlinkVision improves over baseline, while AnthroTAP annotated dataset achieves substantially larger gains despite pseudo-GT labels. Both datasets contain similar human motion patterns, differing primarily in GT accuracy and real-world visual characteristics.

Impact of trajectory complexity and diversity on training. In Table 6, we investigate how trajectory complexity and diversity affect point tracking performance by creating partitioned datasets based on the metrics defined in Table 4. We train LocoTrack on three configurations: baseline, low-complexity trajectories only, and full dataset. Low-complexity trajectories are defined as those below the median angular acceleration value in our dataset. Results show that training on the full dataset, which contains high-complexity and high-diversity trajectories, achieves the largest perfor-



Figure 4: Qualitative comparison of trajectory complexity. Anthro-LD, a dataset generated from our pipeline, exhibits diverse and complex motions, unlike the rigid and simple trajectories found in DriveTrack [3].

Table 6: Analysis of the impact of track diversity and complexity. We evaluate how training with low-diversity and low-complexity tracks affects model performance.

Method	DAVIS		
	AJ	$< \delta_{avg}$	OA
LocoTrack	67.8	79.6	89.9
LocoTrack w/ Least complex tracks	66.0	79.9	86.9
LocoTrack w/ Least diverse tracks	66.6	79.8	87.9
Anthro-LoCoTrack (256×256)	69.0	81.0	90.8

performance gains. Training on low-complexity trajectories alone provides marginal improvements and even decreases performance on certain metrics compared to baseline. This indicates that trajectory complexity and diversity from human motion provide valuable training signals for point tracking models.

Ablation on optical flow based track filtering. In Table 7, we ablate the effect of optical flow-based filtering by comparing it with the baseline that uses trajectories projected from the human mesh and occlusion prediction via ray casting. While the baseline already achieves strong performance, applying trajectory rejection yields a further performance boost.

Visual comparison with DriveTrack [3]. In Figure 4, we

Table 7: Ablation on optical flow based track rejection. Optical flow based rejection helps the model to learn more refined tracks.

Method	DAVIS		
	AJ	$< \delta_{avg}$	OA
Baseline	64.4	76.9	88.6
+ Optical flow based rejection	64.8	77.3	89.1

qualitatively compare our dataset with DriveTrack [3], which is also a point-tracking dataset sourced from real videos. Observing the point traces, DriveTrack mostly exhibits monotonic motion, and the tracks tend to follow similar trajectories because they are concentrated on rigid objects undergoing largely uniform movement. In contrast, our dataset contains highly complex and diverse motion patterns.

5. Conclusion

In this paper, we presented a novel method for generating highly complex pseudo-labeled data for point tracking by leveraging the inherent complexities of human motion captured in videos. By fitting SMPL models to real-world human videos, accurately modeling occlusions via ray-casting, and refining trajectories using optical flow consistency, our approach significantly alleviates the bottleneck of manual annotation. A model trained on our dataset achieves state-

of-the-art results with orders of magnitude less data than existing methods. Our method provides an effective path forward for robust point tracking in real-world scenarios.

Appendix

A. Additional ablations and analyses

Table 8: Ablation on training video length.

	Video Length	DAVIS		
		AJ	$< \delta_{avg}^x$	OA
(I)	24	<u>64.7</u>	76.8	89.4
(II)	48	64.8	77.3	<u>89.1</u>
(III)	64	64.5	<u>77.1</u>	88.9

Ablation on training video length. In Table 8, we investigate the influence of training video length on model performance. For this analysis, we fine-tuned the LocoTrack [12] base model using our annotated videos, experimenting with distinct clip lengths. The results demonstrate that utilizing video clips of 48 frames yields the optimal performance in terms of both AJ and $< \delta_{avg}^x$.

Table 9: Ablation on frame dilation.

	Frame Dilation	DAVIS		
		AJ	$< \delta_{avg}^x$	OA
(I)	1	<u>64.6</u>	76.7	89.6
(II)	2	64.8	77.3	<u>89.1</u>
(III)	3	64.2	<u>76.9</u>	89.0

Ablation on frame dilation. During training, we adjust the frame rate to control the motion speed by sampling video frames with different dilation factors. In Table 9, we test dilations of 1, 2, and 3, corresponding to $1\times$, $2\times$, and $3\times$ faster motion, respectively. When the dilation is too large, the gap between adjacent frames becomes too wide. We found that a dilation factor of 2 yields the best performance in both AJ and $< \delta_{avg}^x$.

Table 10: Ablation on using different amount of extra data.

Method	DAVIS		
	AJ	$< \delta_{avg}^x$	OA
LocoTrack (384 \times 512)	64.8	77.4	86.2
LocoTrack + Ours (250 videos)	65.6	78.5	87.3
LocoTrack + Ours (500 videos)	<u>65.7</u>	<u>78.7</u>	<u>87.2</u>
LocoTrack + Ours (full)	65.9	78.9	87.3

Ablation on training data scale. In Table 10, we examine how the amount of additional training data influences model performance. Starting from our full dataset containing 1.4K videos, we evaluate reduced subsets of 500 and 250 videos. The results show that even when using only a fraction of

the full dataset, our additional videos consistently improve performance over the LocoTrack baseline across all metrics. This demonstrates that our dataset provides strong supervision signals, and meaningful gains can be achieved even with limited data.

Table 11: Ablation on proposed visibility prediction method.

Method	DAVIS		
	AJ	$< \delta_{avg}^x$	OA
LocoTrack (384 \times 512)	<u>64.8</u>	77.4	<u>86.2</u>
LocoTrack + Ours (w/o visibility prediction)	64.6	<u>77.7</u>	85.2
LocoTrack + Ours (full)	65.9	78.9	87.3

Ablation on visibility prediction. In Table 11, we evaluate the impact of our proposed visibility prediction module. Removing the visibility signal results in a performance drop in both AJ and OA, indicating that visibility estimation provides useful supervision during training. The full pipeline with integrated visibility prediction achieves the best performance across all metrics.

B. Additional visualization

We visualize videos annotated using our pipeline in Figure 7 and Figure 8. The visualizations highlight the complex motion present in the dataset.

C. Filtering outlier trajectories with optical flow

While HMR methods [5, 17, 20] have become increasingly robust to challenges such as motion blur, rapid movements, and varying lighting conditions due to their strong human priors, they may still produce occasional errors or inconsistencies in mesh predictions under extreme conditions. Furthermore, our ray-casting-based visibility prediction is limited to occlusions caused by other modeled humans and does not account for occlusions from general scene objects. In addition, the parametric nature of the SMPL model makes it less effective at capturing the motion of highly deformable or loosely attached clothing and accessories.

To mitigate the impact of these potential inaccuracies on our pseudo-labels and thus improve the quality of training data, we introduce an optical flow-based filtering stage, illustrated in Figure 5. Optical flow [24, 59, 66] is particularly well-suited for this task due to its established accuracy in estimating dense motion between adjacent frames. Over very short temporal windows, these flow-based predictions can provide strong local motion cues to validate or identify discrepancies in the HMR-derived trajectories, especially when dealing with complex non-rigid deformations or potential tracking drift [11, 45].

The primary objective of this stage is not to replace the HMR-derived tracks but to identify and remove potentially erroneous segments or entire trajectories. Our goal is to achieve a high true positive rate for valid track segments

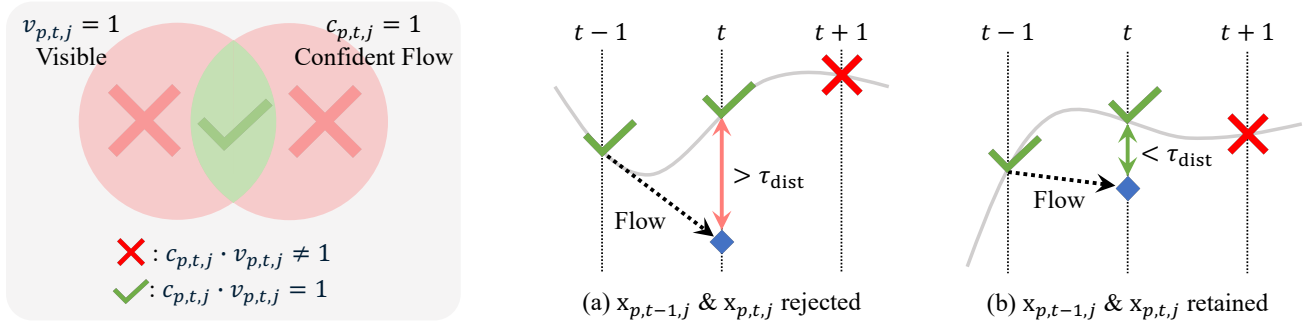


Figure 5: Filtering erroneous tracks with optical flow. We filter trajectories predicted from the human mesh using optical flow. First, we retain points that are both considered visible with ray-casting and have confident optical flow at the predicted position ($c_{p,t,j} \cdot v_{p,t,j} = 1$), denoted as \checkmark . If the difference between the trajectory predicted from the human mesh and the optical flow exceeds a threshold τ_{dist} , the point is considered erroneous, as depicted in (a), otherwise retained as in (b). We omit the normalization process for clarity.

while maintaining a sufficiently high true negative rate for incorrect ones. We operate under the assumption that training a point tracker with a smaller set of highly accurate pseudo-labels is more beneficial than using a larger set contaminated with significant errors.

Identify confident optical flow. For each pair of consecutive frames (I_t, I_{t+1}), we compute both the forward optical flow map from I_t to I_{t+1} , denoted $\mathbf{F}_{t \rightarrow t+1}$, and the backward optical flow map $\mathbf{F}_{t+1 \rightarrow t}$. We use $\mathbf{f}(\mathbf{F}, \mathbf{x})$ to denote the process of sampling the flow vector from map \mathbf{F} at sub-pixel location \mathbf{x} using bilinear interpolation. For notational simplicity, we define:

$$\xi_{p,t,j} = \mathbf{f}(\mathbf{F}_{t \rightarrow t+1}, \mathbf{x}_{p,t,j}), \quad (1)$$

$$\zeta_{p,t,j} = \mathbf{f}(\mathbf{F}_{t+1 \rightarrow t}, \mathbf{x}_{p,t,j} + \xi_{p,t,j}). \quad (2)$$

To assess the reliability of the optical flow estimation itself at a given point $\mathbf{x}_{p,t,j}$, we apply a forward-backward consistency check [43]. Let $c_{p,t,j}$ denote the binary indicator of optical flow reliability at point $\mathbf{x}_{p,t,j}$ in frame I_t . A pixel $\mathbf{x}_{p,t,j}$ is considered to have reliable flow ($c_{p,t,j} = 1$) if the L_2 distance between the point warped to frame $t+1$ and then back to frame t is below a predefined threshold δ_{cons} :

$$c_{p,t,j} = \mathbb{1} [\|\xi_{p,t,j} + \zeta_{p,t,j}\|_2 < \delta_{\text{cons}}]. \quad (3)$$

Find erroneous trajectories. For each point $\mathbf{x}_{p,t,j}$ within a pseudo-labeled trajectory $\mathcal{X}_{p,j}$ (where t and $t+1$ are both in $\mathcal{T}_{p,j}$), we examine the predicted motion to the next frame, $\mathbf{x}_{p,t+1,j}$. The displacement vector derived from the HMR pseudo-label is $\Delta \mathbf{x}_{p,t,j}^{\text{HMR}} = \mathbf{x}_{p,t+1,j} - \mathbf{x}_{p,t,j}$. We compare this to the optical flow displacement $\xi_{p,t,j}$ (previously defined as the forward flow at location $\mathbf{x}_{p,t,j}$).

To compare these two displacement vectors, $\Delta \mathbf{x}_{p,t,j}^{\text{HMR}}$ and $\xi_{p,t,j}$, robustly, especially in cases of large motion, we normalize them. Let $L_{\text{short}} = \min(\|\Delta \mathbf{x}_{p,t,j}^{\text{HMR}}\|_2, \|\xi_{p,t,j}\|_2) + \epsilon_{\text{norm}}$, where ϵ_{norm} is a small positive constant added to pre-

vent division by zero. The normalized vectors are:

$$\Delta \hat{\mathbf{x}}_{p,t,j}^{\text{HMR}} = \frac{\Delta \mathbf{x}_{p,t,j}^{\text{HMR}}}{L_{\text{short}}}, \quad \hat{\xi}_{p,t,j} = \frac{\xi_{p,t,j}}{L_{\text{short}}}. \quad (4)$$

A point transition from frame t to $t+1$ is flagged as potentially erroneous if the L_2 distance between these normalized displacement vectors exceeds a threshold τ_{dist} . We define an indicator variable $e_{p,t,j}$ for this:

$$e_{p,t,j} = \mathbb{1} [\|\Delta \hat{\mathbf{x}}_{p,t,j}^{\text{HMR}} - \hat{\xi}_{p,t,j}\|_2 > \tau_{\text{dist}}]. \quad (5)$$

Trajectory rejection. We observed that query points located on regions not well captured by the SMPL model, such as loose clothing or hair, often result in a large number of transitions being flagged as unreliable. Nonetheless, even in these cases, certain frames may produce transitions that closely follow the predicted motion and pass the consistency check. To robustly filter such trajectories, we evaluate the proportion of transitions that are flagged as erroneous. For a given trajectory $\mathcal{X}_{p,j}$ (defined by the ordered sequence of frame indices $\mathcal{T}_{p,j}$), we calculate the fraction of its transitions that are flagged as erroneous. This ratio, $R_{p,j}$, is computed by summing over all transitions from a frame t_k to its successor t_{k+1} within the sequence $\mathcal{T}_{p,j}$. Only transitions where the point at the starting frame t_k is estimated as visible ($v_{p,t_k,j} = 1$) by ray casting and the optical flow is deemed reliable ($c_{p,t_k,j} = 1$) are included in this calculation:

$$R_{p,j} = \frac{\sum_{k=1}^{|\mathcal{T}_{p,j}|-1} e_{p,t_k,j} \cdot v_{p,t_k,j} \cdot c_{p,t_k,j}}{\sum_{k=1}^{|\mathcal{T}_{p,j}|-1} v_{p,t_k,j} \cdot c_{p,t_k,j} + \epsilon_{\text{ratio}}}. \quad (6)$$

where (t_k, t_{k+1}) denotes the k -th pair of consecutive frame indices in the ordered set $\mathcal{T}_{p,j}$. The term $e_{p,t_k,j}$ indicates that the transition starting at frame t_k (and ending at t_{k+1}) is erroneous. ϵ_{ratio} is a small constant to ensure numerical stability in case the denominator is zero. A trajectory $\mathcal{X}_{p,j}$ is ultimately rejected if this erroneous transition ratio $R_{p,j}$ exceeds a predefined threshold τ_{ratio} .

For trajectories that pass this trajectory-level filtering, any individual point-pair transition ($\mathbf{x}_{p,t,j}, \mathbf{x}_{p,t+1,j}$) still flagged as erroneous ($e_{p,t,j} = 1$) is considered unreliable. For the purpose of training a point tracking model, such individual erroneous transitions are excluded.

D. Trajectory complexity and diversity analysis

To quantitatively evaluate the characteristics of generated pseudo-labeled trajectories $\mathcal{X}_{p,j}$, we employ metrics for trajectory complexity and dataset diversity. These metrics help in understanding the nature of the motion patterns captured. All trajectories are sequences of 2D points $\mathbf{x}_{p,t,j}$ over time t . Calculations are performed on contiguous visible segments of these trajectories, and points are assumed to be normalized by frame dimensions.

Trajectory complexity. Trajectory complexity is quantified using the mean angular acceleration magnitude. This metric captures the rate of change in the direction of motion, highlighting non-linear movements and directional variations. For a given visible segment of a trajectory $\mathcal{X}_{p,j}$, consisting of an ordered sequence of points ($\mathbf{x}_0, \mathbf{x}_1, \dots, \mathbf{x}_K$) (where \mathbf{x}_k corresponds to a point $\mathbf{x}_{p,t_k,j}$ from the trajectory, requiring at least 4 points with $K \geq 3$ for at least one angular acceleration value), and assuming a constant time step Δt between frames:

First, a sequence of velocity vectors \mathbf{u}_k between consecutive points is computed:

$$\mathbf{u}_k = \mathbf{x}_{k+1} - \mathbf{x}_k \quad \text{for } k = 0, \dots, K-1. \quad (7)$$

The signed turning angle θ_k at point \mathbf{x}_{k+1} (i.e., between vectors \mathbf{u}_k and \mathbf{u}_{k+1}) is calculated as:

$$\theta_k = \text{atan2}(\mathbf{u}_k^{(1)} \mathbf{u}_{k+1}^{(2)} - \mathbf{u}_k^{(2)} \mathbf{u}_{k+1}^{(1)}, \mathbf{u}_k \cdot \mathbf{u}_{k+1}), \quad (8)$$

for $k = 0, \dots, K-2$. This sequence of angles is then unwrapped to obtain a continuous sequence of angles $\Phi = (\phi_0, \phi_1, \dots, \phi_{K-2})$ by adding multiples of $\pm 2\pi$ to eliminate jumps. The sequence of angular velocities ω_k is computed from the unwrapped turning angles:

$$\omega_k = \frac{\phi_k}{\Delta t} \quad \text{for } k = 0, \dots, K-2. \quad (9)$$

The angular accelerations α_k are then found by taking the difference between consecutive angular velocities:

$$\alpha_k = \frac{\omega_{k+1} - \omega_k}{\Delta t} \quad \text{for } k = 0, \dots, K-3. \quad (10)$$

The complexity for the segment, C_{seg} , is the mean of the magnitudes of these angular accelerations:

$$C_{\text{seg}} = \frac{1}{K-2} \sum_{k=0}^{K-3} |\alpha_k|. \quad (11)$$

The complexity for an entire trajectory $\mathcal{X}_{p,j}$, denoted $C_{\mathcal{X}_{p,j}}$, is the average of C_{seg} over all its valid visible segments. The overall dataset complexity is the mean of $C_{\mathcal{X}_{p,j}}$ across all trajectories.

Trajectory diversity. Trajectory diversity is assessed by computing the mean standard deviation of centered trajectories from a mean centered trajectory. This measures the spatial variability of trajectories in terms of their shape and relative motion, independent of their absolute starting positions.

Consider a set of N trajectories $\{\mathcal{X}_1, \mathcal{X}_2, \dots, \mathcal{X}_N\}$ within a single video, where \mathcal{X}_i refers to a specific $\mathcal{X}_{p,j}$, and $\mathcal{X}_i(t)$ denotes the 2D coordinate $\mathbf{x}_{p,t,j}$ for the i -th trajectory at frame t . First, each trajectory $\mathcal{X}_i(t)$ is centered by subtracting the coordinates of its first visible point $\mathcal{X}_i(t_{i,\text{first_vis}})$ from all its subsequent visible points. Let this centered trajectory be $\mathcal{X}'_i(t)$:

$$\mathcal{X}'_i(t) = \mathcal{X}_i(t) - \mathcal{X}_i(t_{i,\text{first_vis}}) \quad \text{for visible } t \geq t_{i,\text{first_vis}}. \quad (12)$$

Points where the trajectory is occluded or prior to $t_{i,\text{first_vis}}$ are considered invalid. A mean centered trajectory $M'(t)$ is computed by averaging the coordinates of all valid centered trajectories at each frame t :

$$M'(t) = \frac{1}{|\mathcal{V}_t|} \sum_{i \in \mathcal{V}_t} \mathcal{X}'_i(t). \quad (13)$$

where \mathcal{V}_t is the set of indices of trajectories having valid centered data at frame t . For each centered trajectory \mathcal{X}'_i , the mean squared Euclidean distance (MSD_i) from $M'(t)$ is calculated over all frames $t \in \mathcal{T}_i$ where both $\mathcal{X}'_i(t)$ and $M'(t)$ are valid:

$$MSD_i = \frac{1}{|\mathcal{T}_i|} \sum_{t \in \mathcal{T}_i} \|\mathcal{X}'_i(t) - M'(t)\|_2^2. \quad (14)$$

The standard deviation for trajectory i is then $SD_i = \sqrt{MSD_i}$. The diversity score D_{video} for the video (or dataset) is the mean of these individual trajectory standard deviations:

$$D_{\text{video}} = \text{mean}(SD_1, SD_2, \dots, SD_N). \quad (15)$$

E. Additional data statistics

Statistics on the number of people in training videos. In Figure 6, we investigate the number of people per frame in the generated dataset. Most frames contain more than one person (82%), which can lead to complex trajectories due to occlusions between individuals.

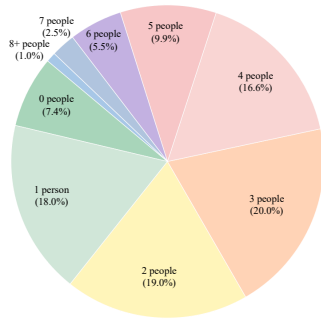


Figure 6: The number of people per frame. Anthro-LD, the dataset generated with our pipeline, contains videos where most scenes include more than one person, contributing to the complexity of the trajectories.

F. Limitations and social impact

While our pseudo-labels show a great performance boost when used to train point tracking models, they are primarily designed to filter out erroneous trajectories. This means that some potentially helpful trajectories might be rejected. Furthermore, visible points in the video could be mistakenly identified as occluded. This inaccuracy regarding occlusion status led us to decide against supervising occlusion directly, and instead focus only on position. Although a dataset with inaccurate occlusion information can still be helpful for training, its utility as a benchmark is limited.

Social impact. This work significantly enhances point tracking accessibility and efficiency by automating data generation, thereby reducing reliance on costly manual annotation and extensive computing. This advancement can benefit robotics, 3D/4D reconstruction, and video editing. Open-sourcing the dataset and pipeline will promote collaborative research of point tracking. While not explicitly discussed, potential misuse for surveillance should be considered.

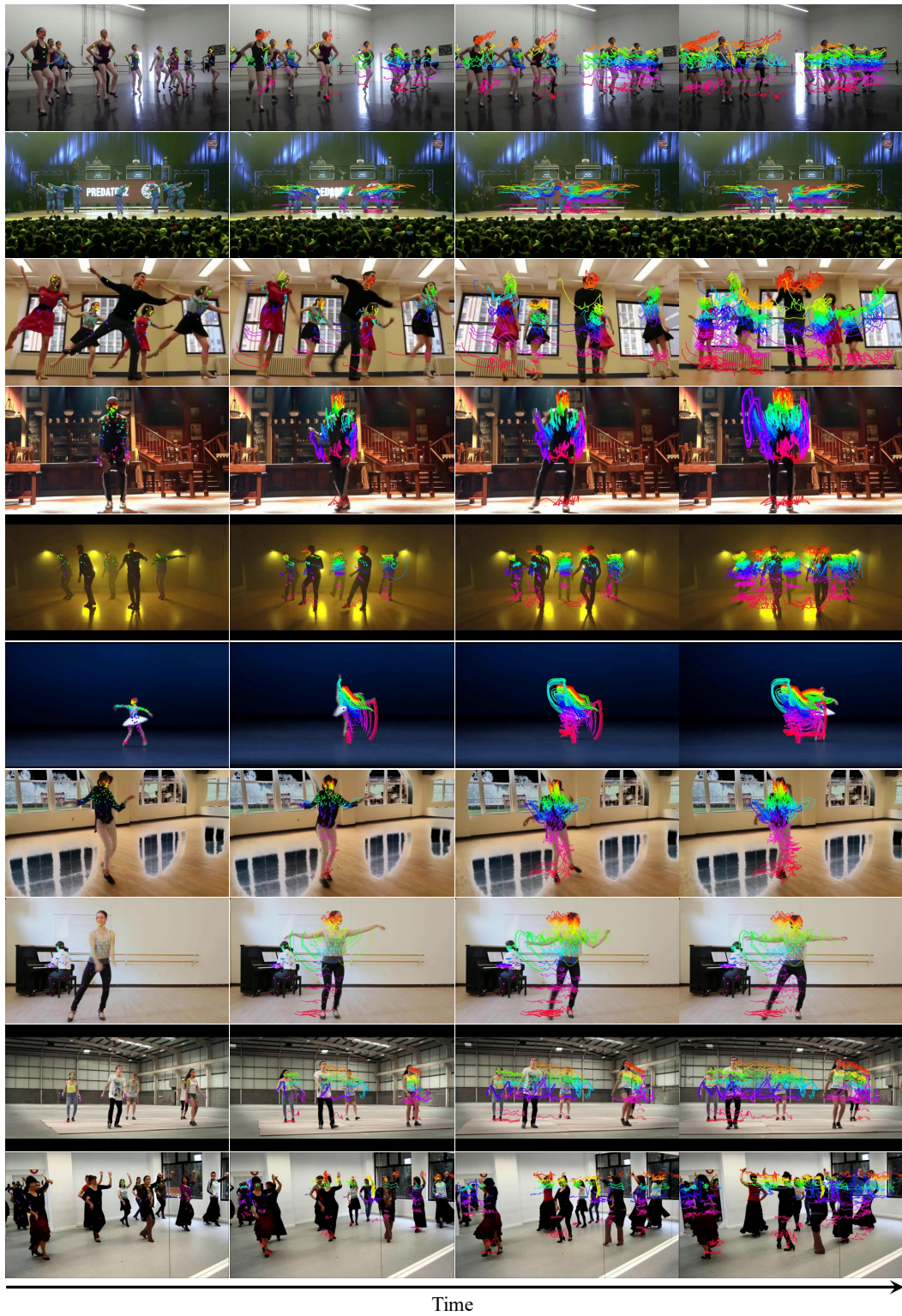


Figure 7: Additional visualization of videos annotated with our pipeline. In this example, we visualize trajectories extracted using our pipeline.



Figure 8: Additional visualization of videos annotated with our pipeline. In this example, we visualize trajectories extracted using our pipeline.

References

- [1] Görkay Aydemir, Xiongyi Cai, Weidi Xie, and Fatma Güney. Track-on: Transformer-based online point tracking with memory. *arXiv preprint arXiv:2501.18487*, 2025. 2, 5
- [2] Abhishek Badki, Hang Su, Bowen Wen, and Orazio Gallo. L4P: Towards unified low-level 4D vision perception. In *International Conference on 3D Vision (3DV)*, 2026. 1
- [3] Arjun Balasingam, Joseph Chandler, Chenning Li, Zhoutong Zhang, and Hari Balakrishnan. Drivetrack: A benchmark for long-range point tracking in real-world videos. In *Proceedings of the IEEE/CVF Conference on Computer Vision and Pattern Recognition*, pages 22488–22497, 2024. 2, 7, 8
- [4] Homanga Bharadhwaj, Roozbeh Mottaghi, Abhinav Gupta, and Shubham Tulsiani. Track2act: Predicting point tracks from internet videos enables generalizable robot manipulation. In *European Conference on Computer Vision*, pages 306–324. Springer, 2024. 1
- [5] Michael J Black, Priyanka Patel, Joachim Tesch, and Jionglong Yang. Bedlam: A synthetic dataset of bodies exhibiting detailed lifelike animated motion. In *Proceedings of the IEEE/CVF Conference on Computer Vision and Pattern Recognition*, pages 8726–8737, 2023. 9
- [6] Federica Bogo, Angjoo Kanazawa, Christoph Lassner, Peter Gehler, Javier Romero, and Michael J Black. Keep it smpl: Automatic estimation of 3d human pose and shape from a single image. In *Computer Vision—ECCV 2016: 14th European Conference, Amsterdam, The Netherlands, October 11–14, 2016, Proceedings, Part V 14*, pages 561–578. Springer, 2016. 3
- [7] Zhe Cao, Tomas Simon, Shih-En Wei, and Yaser Sheikh. Realtime multi-person 2d pose estimation using part affinity fields. In *Proceedings of the IEEE conference on computer vision and pattern recognition*, pages 7291–7299, 2017. 3
- [8] Daniel Castro, Steven Hickson, Patsorn Sangkloy, Bhavishya Mittal, Sean Dai, James Hays, and Irfan Essa. Let’s dance: Learning from online dance videos. *arXiv preprint arXiv:1801.07388*, 2018. 5, 6, 7
- [9] Weirong Chen, Le Chen, Rui Wang, and Marc Pollefeys. Leap-vo: Long-term effective any point tracking for visual odometry. In *Proceedings of the IEEE/CVF Conference on Computer Vision and Pattern Recognition*, pages 19844–19853, 2024. 1
- [10] Bowen Cheng, Ishan Misra, Alexander G. Schwing, Alexander Kirillov, and Rohit Girdhar. Masked-attention mask transformer for universal image segmentation. *arXiv*, 2021. 6
- [11] Seokju Cho, Jiahui Huang, Seungryong Kim, and Joon-Young Lee. Flowtrack: Revisiting optical flow for long-range dense tracking. In *Proceedings of the IEEE/CVF Conference on Computer Vision and Pattern Recognition*, pages 19268–19277, 2024. 2, 3, 9
- [12] Seokju Cho, Jiahui Huang, Jisu Nam, Honggyu An, Seungryong Kim, and Joon-Young Lee. Local all-pair correspondence for point tracking. In *European Conference on Computer Vision*, pages 306–325. Springer, 2024. 1, 2, 4, 5, 6, 9
- [13] Seokju Cho, Jiahui Huang, Seungryong Kim, and Joon-Young Lee. Seurat: From moving points to depth. *arXiv preprint arXiv:2504.14687*, 2025. 2
- [14] Carl Doersch, Ankush Gupta, Larisa Markeeva, Adria Recasens, Lucas Smaira, Yusuf Aytar, Joao Carreira, Andrew Zisserman, and Yi Yang. Tap-vid: A benchmark for tracking any point in a video. *Advances in Neural Information Processing Systems*, 35:13610–13626, 2022. 1, 2, 3, 5, 7
- [15] Carl Doersch, Yi Yang, Mel Vecerik, Dilara Gokay, Ankush Gupta, Yusuf Aytar, Joao Carreira, and Andrew Zisserman. Tapir: Tracking any point with per-frame initialization and temporal refinement. In *Proceedings of the IEEE/CVF International Conference on Computer Vision*, pages 10061–10072, 2023. 2, 5
- [16] Carl Doersch, Pauline Luc, Yi Yang, Dilara Gokay, Skanda Koppula, Ankush Gupta, Joseph Heyward, Ignacio Rocco, Ross Goroshin, João Carreira, et al. Bootstrap: Bootstrapped training for tracking-any-point. In *Proceedings of the Asian Conference on Computer Vision*, pages 3257–3274, 2024. 1, 2, 3, 5, 6
- [17] Sai Kumar Dwivedi, Yu Sun, Priyanka Patel, Yao Feng, and Michael J Black. Tokenhmr: Advancing human mesh recovery with a tokenized pose representation. In *Proceedings of the IEEE/CVF Conference on Computer Vision and Pattern Recognition*, pages 1323–1333, 2024. 2, 3, 4, 5, 9
- [18] Haiwen Feng, Junyi Zhang, Qianqian Wang, Yufei Ye, Pengcheng Yu, Michael J. Black, Trevor Darrell, and Angjoo Kanazawa. St4rtrack: Simultaneous 4d reconstruction and tracking in the world. *arXiv preprint arxiv:2504.13152*, 2025. 1
- [19] Daniel Geng, Charles Herrmann, Junhwa Hur, Forrester Cole, Serena Zhang, Tobias Pfaff, Tatiana Lopez-Guevara, Carl Doersch, Yusuf Aytar, Michael Rubinstein, et al. Motion prompting: Controlling video generation with motion trajectories. *arXiv preprint arXiv:2412.02700*, 2024. 1
- [20] Shubham Goel, Georgios Pavlakos, Jathushan Rajasegaran, Angjoo Kanazawa, and Jitendra Malik. Humans in 4d: Reconstructing and tracking humans with transformers. In *Proceedings of the IEEE/CVF International Conference on Computer Vision*, pages 14783–14794, 2023. 3, 9
- [21] Klaus Greff, Francois Belletti, Lucas Beyer, Carl Doersch, Yilun Du, Daniel Duckworth, David J Fleet, Dan Gnanaprasam, Florian Golemo, Charles Herrmann, et al. Kubric: A scalable dataset generator. In *Proceedings of the IEEE/CVF conference on computer vision and pattern recognition*, pages 3749–3761, 2022. 1, 2, 3, 5, 7
- [22] Adam W Harley, Zhaoyuan Fang, and Katerina Fragkiadaki. Particle video revisited: Tracking through occlusions using point trajectories. In *European Conference on Computer Vision*, pages 59–75. Springer, 2022. 1, 2, 5
- [23] Nan Huang, Wenzhao Zheng, Chenfeng Xu, Kurt Keutzer, Shanghang Zhang, Angjoo Kanazawa, and Qianqian Wang. Segment any motion in videos, 2025. 1
- [24] Zhaoyang Huang, Xiaoyu Shi, Chao Zhang, Qiang Wang, Ka Chun Cheung, Hongwei Qin, Jifeng Dai, and Hongsheng Li. Flowformer: A transformer architecture for optical flow. In *European conference on computer vision*, pages 668–685. Springer, 2022. 9
- [25] Hyeonho Jeong, Chun-Hao Paul Huang, Jong Chul Ye, Niloy Mitra, and Duygu Ceylan. Track4gen: Teaching video diffu-

- sion models to track points improves video generation. *arXiv preprint arXiv:2412.06016*, 2024. 1
- [26] Nikita Karaev, Ignacio Rocco, Benjamin Graham, Natalia Neverova, Andrea Vedaldi, and Christian Rupprecht. Dynamicstereo: Consistent dynamic depth from stereo videos. In *Proceedings of the IEEE/CVF Conference on Computer Vision and Pattern Recognition*, pages 13229–13239, 2023. 3
- [27] Nikita Karaev, Iurii Makarov, Jianyuan Wang, Natalia Neverova, Andrea Vedaldi, and Christian Rupprecht. Co-tracker3: Simpler and better point tracking by pseudo-labelling real videos. *arXiv preprint arXiv:2410.11831*, 2024. 1, 2, 3, 4, 5, 6, 7
- [28] Nikita Karaev, Ignacio Rocco, Benjamin Graham, Natalia Neverova, Andrea Vedaldi, and Christian Rupprecht. Co-tracker: It is better to track together. In *European Conference on Computer Vision*, pages 18–35. Springer, 2024. 1, 2, 5
- [29] Laurynas Karazija, Iro Laina, Christian Rupprecht, and Andrea Vedaldi. Learning segmentation from point trajectories, 2024. 1
- [30] Yoni Kasten, Wuyue Lu, and Haggai Maron. Fast encoder-based 3d from casual videos via point track processing. In *The Thirty-eighth Annual Conference on Neural Information Processing Systems*. 1
- [31] Will Kay, Joao Carreira, Karen Simonyan, Brian Zhang, Chloe Hillier, Sudheendra Vijayanarasimhan, Fabio Viola, Tim Green, Trevor Back, Paul Natsev, et al. The kinetics human action video dataset. *arXiv preprint arXiv:1705.06950*, 2017. 2, 6
- [32] Inès Hyeonsu Kim, Seokju Cho, Jiahui Huang, Jung Yi, Joon-Young Lee, and Seungryong Kim. Exploring temporally-aware features for point tracking. *arXiv preprint arXiv:2501.12218*, 2025. 2
- [33] Christoph Lassner, Javier Romero, Martin Kiefel, Federica Bogo, Michael J Black, and Peter V Gehler. Unite the people: Closing the loop between 3d and 2d human representations. In *Proceedings of the IEEE conference on computer vision and pattern recognition*, pages 6050–6059, 2017. 3
- [34] Guillaume Le Moing, Jean Ponce, and Cordelia Schmid. Dense optical tracking: Connecting the dots. In *CVPR*, 2024. 2
- [35] Alex X Lee, Coline Manon Devin, Yuxiang Zhou, Thomas Lampe, Konstantinos Bousmalis, Jost Tobias Springenberg, Arunkumar Byravan, Abbas Abdolmaleki, Nimrod Gileadi, David Khosid, et al. Beyond pick-and-place: Tackling robotic stacking of diverse shapes. In *5th Annual Conference on Robot Learning*, 2021. 2
- [36] Hongyang Li, Hao Zhang, Shilong Liu, Zhaoyang Zeng, Feng Li, Bohan Li, Tianhe Ren, and Lei Zhang. Taptrv2: Attention-based position update improves tracking any point. *Advances in Neural Information Processing Systems*, 37: 101074–101095, 2024. 2, 5
- [37] Hongyang Li, Hao Zhang, Shilong Liu, Zhaoyang Zeng, Tianhe Ren, Feng Li, and Lei Zhang. Taptr: Tracking any point with transformers as detection. In *European Conference on Computer Vision*, pages 57–75. Springer, 2024. 2, 5
- [38] Yijin Li, Yichen Shen, Zhaoyang Huang, Shuo Chen, Weikang Bian, Xiaoyu Shi, Fu-Yun Wang, Keqiang Sun, Hujun Bao, Zhaopeng Cui, et al. Blinkvision: A benchmark for optical flow, scene flow and point tracking estimation using rgb frames and events. In *European Conference on Computer Vision*, pages 19–36. Springer, 2024. 7
- [39] Matthew Loper, Naureen Mahmood, Javier Romero, Gerard Pons-Moll, and Michael J. Black. SMPL: A skinned multi-person linear model. *ACM Trans. Graphics (Proc. SIGGRAPH Asia)*, 34(6):248:1–248:16, 2015. 3
- [40] Matthew Loper, Naureen Mahmood, Javier Romero, Gerard Pons-Moll, and Michael J Black. Smpl: A skinned multi-person linear model. In *Seminal Graphics Papers: Pushing the Boundaries, Volume 2*, pages 851–866, 2023. 3
- [41] Ilya Loshchilov and Frank Hutter. Decoupled weight decay regularization. *arXiv preprint arXiv:1711.05101*, 2017. 5
- [42] Nikolaus Mayer, Eddy Ilg, Philip Hausser, Philipp Fischer, Daniel Cremers, Alexey Dosovitskiy, and Thomas Brox. A large dataset to train convolutional networks for disparity, optical flow, and scene flow estimation. In *Proceedings of the IEEE conference on computer vision and pattern recognition*, pages 4040–4048, 2016. 1, 2, 3, 5
- [43] Simon Meister, Junhwa Hur, and Stefan Roth. Unflow: Unsupervised learning of optical flow with a bidirectional census loss. In *Proceedings of the AAAI conference on artificial intelligence*, 2018. 2, 3, 10
- [44] Tomas Möller and Ben Trumbore. Fast, minimum storage ray/triangle intersection. In *ACM SIGGRAPH 2005 Courses*, pages 7–es. 2005. 4
- [45] Michal Neoral, Jonáš Šerých, and Jiří Matas. Mft: Long-term tracking of every pixel. In *Proceedings of the IEEE/CVF Winter Conference on Applications of Computer Vision (WACV)*, pages 6837–6847, 2024. 9
- [46] Maxime Oquab, Timothée Darcet, Théo Moutakanni, Huy Vo, Marc Szafraniec, Vasil Khalidov, Pierre Fernandez, Daniel Haziza, Francisco Massa, Alaaeldin El-Nouby, et al. Dinov2: Learning robust visual features without supervision. *arXiv preprint arXiv:2304.07193*, 2023. 2
- [47] F. Perazzi, J. Pont-Tuset, B. McWilliams, L. Van Gool, M. Gross, and A. Sorkine-Hornung. A benchmark dataset and evaluation methodology for video object segmentation. In *Computer Vision and Pattern Recognition*, 2016. 6
- [48] Jordi Pont-Tuset, Federico Perazzi, Sergi Caelles, Pablo Arbeláez, Alex Sorkine-Hornung, and Luc Van Gool. The 2017 davis challenge on video object segmentation. *arXiv preprint arXiv:1704.00675*, 2017. 2, 6
- [49] Jinyuan Qu, Hongyang Li, Shilong Liu, Tianhe Ren, Zhaoyang Zeng, and Lei Zhang. Taptrv3: Spatial and temporal context foster robust tracking of any point in long video. *arXiv preprint arXiv:2411.18671*, 2024. 2, 5
- [50] Xuanchi Ren, Tianchang Shen, Jiahui Huang, Huan Ling, Yifan Lu, Merlin Nimier-David, Thomas Müller, Alexander Keller, Sanja Fidler, and Jun Gao. Gen3c: 3d-informed world-consistent video generation with precise camera control. *arXiv preprint arXiv:2503.03751*, 2025. 2
- [51] Chris Rockwell, Joseph Tung, Tsung-Yi Lin, Ming-Yu Liu, David F. Fouhey, and Chen-Hsuan Lin. Dynamic camera poses and where to find them. In *CVPR*, 2025. 1
- [52] Mehdi SM Sajjadi, Henning Meyer, Etienne Pot, Urs Bergmann, Klaus Greff, Noha Radwan, Suhani Vora, Mario

- Lučić, Daniel Duckworth, Alexey Dosovitskiy, et al. Scene representation transformer: Geometry-free novel view synthesis through set-latent scene representations. In *Proceedings of the IEEE/CVF Conference on Computer Vision and Pattern Recognition*, pages 6229–6238, 2022. [2](#)
- [53] Jenny Seidenschwarz, Qunjie Zhou, Bardienus Duisterhof, Deva Ramanan, and Laura Leal-Taixé. Dymomo: Online point tracking by dynamic online monocular gaussian reconstruction. *arXiv preprint arXiv:2409.02104*, 2024. [1](#)
- [54] Ayush Shrivastava and Andrew Owens. Self-supervised any-point tracking by contrastive random walks. 2024. [1](#)
- [55] Gautam Singh, Yi-Fu Wu, and Sungjin Ahn. Simple unsupervised object-centric learning for complex and naturalistic videos. *Advances in Neural Information Processing Systems*, 35:18181–18196, 2022. [2](#)
- [56] Kihyuk Sohn, David Berthelot, Nicholas Carlini, Zizhao Zhang, Han Zhang, Colin A Raffel, Ekin Dogus Cubuk, Alexey Kurakin, and Chun-Liang Li. Fixmatch: Simplifying semi-supervised learning with consistency and confidence. *Advances in neural information processing systems*, 33:596–608, 2020. [1](#)
- [57] Pei Sun, Henrik Kretzschmar, Xerxes Dotiwalla, Aurelien Chouard, Vijaysai Patnaik, Paul Tsui, James Guo, Yin Zhou, Yuning Chai, Benjamin Caine, Vijay Vasudevan, Wei Han, Jiquan Ngiam, Hang Zhao, Aleksei Timofeev, Scott Etinger, Maxim Krivokon, Amy Gao, Aditya Joshi, Yu Zhang, Jonathon Shlens, Zhifeng Chen, and Dragomir Anguelov. Scalability in perception for autonomous driving: Waymo open dataset. In *Proceedings of the IEEE/CVF Conference on Computer Vision and Pattern Recognition (CVPR)*, 2020. [3](#)
- [58] Peize Sun, Jinkun Cao, Yi Jiang, Zehuan Yuan, Song Bai, Kris Kitani, and Ping Luo. Dancetrack: Multi-object tracking in uniform appearance and diverse motion. *arXiv preprint arXiv:2111.14690*, 2021. [1](#)
- [59] Zachary Teed and Jia Deng. Raft: Recurrent all-pairs field transforms for optical flow. In *Computer Vision—ECCV 2020: 16th European Conference, Glasgow, UK, August 23–28, 2020, Proceedings, Part II 16*, pages 402–419. Springer, 2020. [2](#), [4](#), [9](#)
- [60] Narek Tumanyan, Assaf Singer, Shai Bagon, and Tali Dekel. Dino-tracker: Taming dino for self-supervised point tracking in a single video. In *European Conference on Computer Vision*, pages 367–385. Springer, 2024. [5](#)
- [61] Mel Vecerik, Carl Doersch, Yi Yang, Todor Davchev, Yusuf Aytar, Guangyao Zhou, Raia Hadsell, Lourdes Agapito, and Jon Scholz. Robotap: Tracking arbitrary points for few-shot visual imitation. In *2024 IEEE International Conference on Robotics and Automation (ICRA)*, pages 5397–5403. IEEE, 2024. [1](#), [5](#)
- [62] Jianyuan Wang, Nikita Karaev, Christian Rupprecht, and David Novotny. Vggsfm: Visual geometry grounded deep structure from motion. In *Proceedings of the IEEE/CVF Conference on Computer Vision and Pattern Recognition*, pages 21686–21697, 2024. [1](#)
- [63] Jianyuan Wang, Minghao Chen, Nikita Karaev, Andrea Vedaldi, Christian Rupprecht, and David Novotny. Vggt: Visual geometry grounded transformer. In *Proceedings of the IEEE/CVF Conference on Computer Vision and Pattern Recognition*, 2025. [1](#)
- [64] Qianqian Wang, Yen-Yu Chang, Ruojin Cai, Zhengqi Li, Bharath Hariharan, Aleksander Holynski, and Noah Snavely. Tracking everything everywhere all at once. In *Proceedings of the IEEE/CVF International Conference on Computer Vision*, pages 19795–19806, 2023. [5](#)
- [65] Qianqian Wang, Vickie Ye, Hang Gao, Jake Austin, Zhengqi Li, and Angjoo Kanazawa. Shape of motion: 4d reconstruction from a single video. *arXiv preprint arXiv:2407.13764*, 2024. [1](#)
- [66] Yihan Wang, Lahav Lipson, and Jia Deng. Sea-raft: Simple, efficient, accurate raft for optical flow. In *European Conference on Computer Vision*, pages 36–54. Springer, 2024. [3](#), [5](#), [9](#)
- [67] Chuan Wen, Xingyu Lin, John So, Kai Chen, Qi Dou, Yang Gao, and Pieter Abbeel. Any-point trajectory modeling for policy learning, 2024. [1](#)
- [68] Yuxi Xiao, Qianqian Wang, Shangzhan Zhang, Nan Xue, Sida Peng, Yujun Shen, and Xiaowei Zhou. Spatialtracker: Tracking any 2d pixels in 3d space. In *Proceedings of the IEEE/CVF Conference on Computer Vision and Pattern Recognition (CVPR)*, pages 20406–20417, 2024. [2](#)
- [69] Yufei Xu, Jing Zhang, Qiming Zhang, and Dacheng Tao. Vit-pose: Simple vision transformer baselines for human pose estimation. *Advances in neural information processing systems*, 35:38571–38584, 2022. [3](#)
- [70] Jianwei Yang, Reuben Tan, Qianhui Wu, Ruijie Zheng, Baolin Peng, Yongyuan Liang, Yu Gu, Mu Cai, Seonghyeon Ye, Joel Jang, et al. Magma: A foundation model for multimodal ai agents. *arXiv preprint arXiv:2502.13130*, 2025. [1](#)
- [71] Yang Zheng, Adam W Harley, Bokui Shen, Gordon Wetzstein, and Leonidas J Guibas. Pointodyssey: A large-scale synthetic dataset for long-term point tracking. In *Proceedings of the IEEE/CVF International Conference on Computer Vision*, pages 19855–19865, 2023. [1](#), [2](#), [3](#), [7](#)